

Numerical simulation of bus aerodynamics on several classes of bridge decks

A. Alonso-Estébanez, J. J. Del Coz Díaz, F. P. Álvarez Rabanal & P. Pascual-Muñoz

To cite this article: A. Alonso-Estébanez, J. J. Del Coz Díaz, F. P. Álvarez Rabanal & P. Pascual-Muñoz (2017) Numerical simulation of bus aerodynamics on several classes of bridge decks, *Engineering Applications of Computational Fluid Mechanics*, 11:1, 435-449, DOI: [10.1080/19942060.2016.1201544](https://doi.org/10.1080/19942060.2016.1201544)

To link to this article: <https://doi.org/10.1080/19942060.2016.1201544>



© 2016 The Author(s). Published by Informa UK Limited, trading as Taylor & Francis Group



Published online: 18 Jul 2016.



Submit your article to this journal [↗](#)



Article views: 951



View related articles [↗](#)



View Crossmark data [↗](#)

Numerical simulation of bus aerodynamics on several classes of bridge decks

A. Alonso-Estébanez ^a, J. J. Del Coz Díaz ^b, F. P. Álvarez Rabanal ^b and P. Pascual-Muñoz ^a

^aDepartment of Transport, Project and Process Technology, University of Cantabria, Santander, Spain; ^bDepartment of Construction, GICONSIME Research Team, University of Oviedo, Gijón, Spain

ABSTRACT

This paper is focused on improving traffic safety on bridges under crosswind conditions, as adverse wind conditions can increase the risk of traffic accidents. Two ways to improve traffic safety are investigated: improving vehicle stability by means of wind fences installed on the bridge deck and by modifying the design parameters of the infrastructure. Specifically, this study examines the influence of different parameters related to the bridge deck configuration on the aerodynamic coefficients acting on a bus model under crosswind conditions. The aerodynamic coefficients related to side force, lift force and rollover moment are obtained for three classes of bridge deck (box, girder and board) by numerical simulation. FLUENT was used to solve the Reynolds-averaged Navier–Stokes (RANS) equations along with the shear stress transport (SST) $k-\omega$ turbulence model. Two crash barriers located on the box bridge deck were replaced with an articulating wind fence model and the effect of the angle between the wind fence and the horizontal plane on the bus aerodynamic was investigated. The risk of rollover accidents was found to be slightly influenced by the bridge deck type for a yaw angle range between 75° and 120°. In order to study the effect of the yaw angle on the aerodynamic coefficients acting on bus, both the bus model and the bridge model were simultaneously rotated. The minimum value of the rollover coefficient was obtained for an angle of 60° between the wind fence slope and the horizontal plane. The only geometry parameter of the box bridge deck which significantly affects bus aerodynamics is the box height. The present research highlights the usefulness of computational fluid dynamics (CFD) for improving traffic safety, studying the performance of the articulating wind fence, and determining which geometry parameters of the box deck have a significant influence on the bus stability.

ARTICLE HISTORY

Received 20 November 2015
Accepted 24 May 2016

KEYWORDS

Crosswind; bridge decks;
heavy vehicle aerodynamics;
finite-volume method (FVM);
computational fluid
dynamics (CFD)

1. Introduction

Wind conditions around locations such as bridges and viaducts may have an especially negative impact on vehicle stability. Particularly, the control of high-sided vehicles requires more attention because they are more susceptible to rollover or lane-changing accidents (Baker & Reynolds, 1992; Dorigatti et al., 2012). Nevertheless, in Cheung and Chan (2010), it is demonstrated that lightweight vehicles are also likely to suffer impaired handling while driving across bridges even when exposed to relatively low wind velocities. Nowadays, some authorities around the world opt to close bridges when the wind velocity exceeds a set threshold. In some cases this wind velocity threshold is based on previous experience rather than being the result of a quantitative procedure that better guarantees user safety.

The interruption of traffic on some bridges may result in huge economic losses, especially if the bridges are integral to local market logistics. Therefore, viaducts and bridges that are routinely exposed to crosswind

conditions can be the cause of both safety and economic issues. As a consequence, several studies have investigated the impact of crosswinds on bridges (Wang, Xu, Zhu, Cao, & Li, 2013; Wang, Xu, Zhu, & Li, 2014). Some studies have focused on the development of procedures to regulate traffic (Cheung & Chan, 2010; Guo & Xu, 2006), while other research has studied wind fence efficiency (Kozmar, Procino, Borsani, & Bartoli, 2012; Rocchi, Rosa, Sabbioni, Sbrosi, & Belloli, 2012). Improving knowledge about the aerodynamic behavior of wind fences located on bridge decks is necessary, since many researchers have focused on the design of wind fences located on the ground the wind conditions are different (Chen, Wang, Sun, & Li, 2012; Judd, Raupach, & Finnigan, 1996).

Another aspect studied is the huge impact of wind conditions (wind velocity, approaching turbulence, wind direction, etc.) on vehicle stability. Kozmar et al. (2012) highlight that high-sided vehicles suffer higher wind loads because the angle formed by the wind direction and the horizontal line in a vertical plane is increased.

CONTACT A. Alonso-Estébanez  alonsoea@unican.es

Charuvisit, Kimura, and Fujino (2004) indicate that an increase in wind velocity reduces the driver's comfort and that the worst value of the horizontal angle formed by the wind direction and normal to bridge direction is 30° for the stability of vehicles. However, Bettle, Holloway, and Venart (2003) particularized the most critical wind direction for the windward and leeward lanes as 90° and 56.3° , respectively. Another wind characteristic which should be considered when evaluating the risk of accident on the roads is the presence of wind gusts because of their negative influence on vehicle stability (Kozmar, Butler, & Kareem, 2009).

Vehicles suffer huge instabilities under crosswind conditions (Argentini, Ozkan, Rocchi, Rosa, & Zasso, 2011; Wang et al., 2014) at the towers on the bridges. In Charuvisit et al. (2004) the effect of tower geometry on vehicle stability was studied. The maximum yawing acceleration on the vehicle was higher for one of the tower models, so some modifications in tower design could benefit traffic safety. Another aspect of bridge design that can affect vehicle stability is the bridge deck model's geometry (Dorigatti et al., 2012; Suzuki, Tanemoto, & Maeda, 2003). In Dorigatti et al. (2012), the aerodynamic coefficients of three types of vehicles (van, truck and bus) were obtained for two bridge deck models, and the bus stability was found to be sensitive to the different geometries. Suzuki et al. (2003) found that an increase in the thickness of a bridge girder also causes the aerodynamic side force coefficient of vehicles to rise. Cheli, Corradi, Rocchi, Tomasini, and Maestrini (2010) and Bettle et al. (2003) obtained the aerodynamic loads acting on vehicles located in the windward lane and the leeward lane. In both studies, the results indicate that aerodynamic loads are higher when vehicles are traveling closer to the windward edge of the deck. Specifically, the rollover moment in the leeward lane was found to be 30% lower than in the windward lane. To carry out these studies, the most frequently used techniques are numerical simulation computational fluid dynamics (CFD), wind tunnel tests and full-scale experiments (Bettle et al., 2003; Cheli, Corradi, Sabbioni, & Tomasini, 2011; Hibino, Shimomura, & Tanifuji, 2010). In many cases the results from numerical simulations are contrasted with the other techniques (Sterling et al., 2010; Sun, Zhang, Guo, Yang, & Liu, 2014).

This study has been proposed to help authorities better manage traffic safety on bridges under adverse crosswind conditions. With this aim in mind, the following objectives are proposed:

- Identify which type of bridge deck most adversely affects bus aerodynamics.

- Obtain the relationship between the angle of the wind fence slope and the aerodynamic coefficient acting on the bus model when it is located on a bridge.
- Determine whether or not it is possible to reduce the aerodynamic coefficients of the bus by modifying the design parameters of a bridge deck.

To achieve these objectives, 3D CFD numerical simulations were carried out in order to study the stability of a 1:40 scale model comprising of a bus on a bridge under crosswind conditions. During this study, the main difficulties arose when setting the grid parameters, selecting one turbulence model between the options provided by FLUENT and proposing the most interesting study cases. In order to overcome these difficulties, on the one hand several numerical models with different grid sizes and turbulence models were solved and, on the other hand, investigations were conducted which focused on the effect of crosswind conditions on traffic safety in bridge decks (Dorigatti et al., 2012; Wang et al., 2013, 2014).

In section 2, both the numerical setup and the mathematical method used to solve the studied cases are defined. Then, in section 3, the procedure used both to select the turbulence model and to define the grid size setup is presented with reference to experimental data (Dorigatti et al., 2012). In section 4, the geometric parameters of a bridge deck with a box are defined and studied by using surface response methodology along with the design of experiment (DOE) technique. In section 5, the results of bus aerodynamics and flow behavior around bridge decks and an articulating wind fence are indicated and discussed. In the last section, the main conclusions from the results of this study are explained.

2. Numerical method

All numerical models were solved by using the CFD software Ansys FLUENT. The geometries for the bus and the bridge decks in this study are now presented.

2.1. Bridge decks and aerodynamic loads

The influence of the bridge deck typology on vehicle stability was studied by obtaining the aerodynamic coefficients from the bus model. Among the types of bridge deck sections built nowadays, the following three were proposed for this study: box, board, and girder (Figure 1). The aerodynamic coefficients acting on the bus located on the bridge decks were obtained for four yaw angle values: 75° , 90° , 105° and 120° . Detailed information about the dimensions of both the bus and the box bridge deck

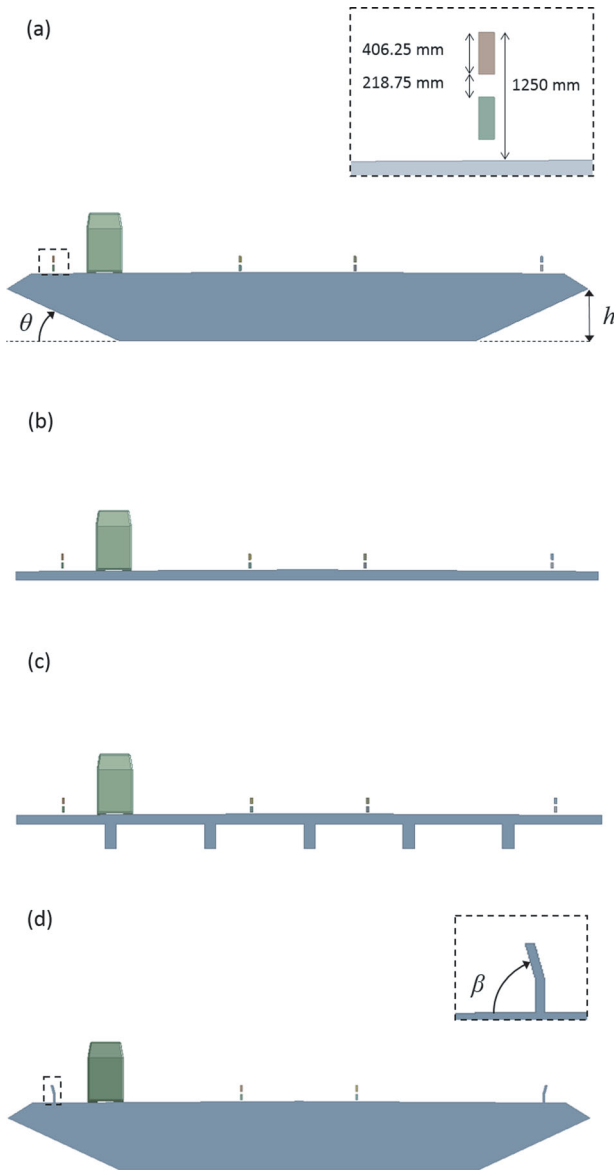


Figure 1. The bridge deck configurations used in this study: (a) box, (b) board, (c) girder, and (d) box with solid fence.

(model scale 1:40) can be found in Dorigatti et al. (2012). This experimental study in the wind tunnel was used to define the numerical setup parameters and then this setup was applied to the other cases proposed in this

study. Four crash barriers which are 1250 mm high at full scale and have a porosity (ratio between open area and total area projected on the normal plane to wind direction) of approximately 35% were installed on the three types of bridge deck. These barriers are composed of two strips with a width of 406.25 mm and a gap between them of 218.75 mm in full scale. An additional model was built for the box bridge deck in which two of the crash barriers were replaced by solid and articulating wind fences (porosity 0%). The wind fence model was divided into two parts of equal length, but the slope angle of the upper part varied with the road plane while the lower part was kept in the vertical position (90° to the road plane) for all cases. Specifically, five values of slope angle β between 60° and 120° were studied. In the vertical position, the articulating wind fence is the same height as the crash barrier. Furthermore, the effect of the box deck design parameters (Figure 1(a)) on the aerodynamic loads acting on the bus was studied by applying the response surface methodology.

On the other hand, the aerodynamic loads and moments acting on the bus obtained are the side force F_S , lift force F_L and rollover moment M_R (Figure 2). The moments caused by side force and lift force were obtained by integrating the pressure about the origin of the reference system (point O in Figure 2) due to wind force components acting on the x -axis and y -axis, respectively. The rollover moment was calculated by adding the moments caused by the side and lift forces. Then, these aerodynamic loads were converted into non-dimensional coefficients using the following equations:

$$C_S = \frac{F_S}{\frac{1}{2}\rho U^2 A_S} \quad (1)$$

$$C_L = \frac{F_L}{\frac{1}{2}\rho U^2 A_S} \quad (2)$$

$$C_R = \frac{M_R}{\frac{1}{2}\rho U^2 A_S H} \quad (3)$$

where ρ is the air density (1.18 kg/m^3), A_S is the side area of the bus ($27,830 \text{ mm}^2$ in the scale model), H is the

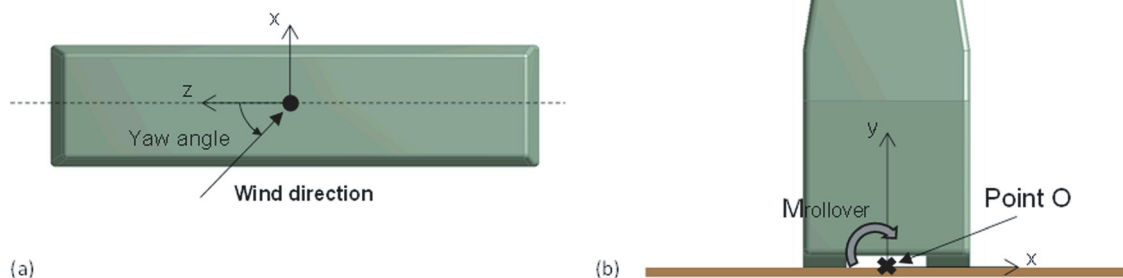


Figure 2. Sign convention for forces, moment and origin of the coordinates reference system.

height of the bus (110 mm in the scale model) and U is the undisturbed wind speed measured 7 m upstream of the bridge deck section model.

2.2. Mathematical approach

The lower region of the atmosphere where the transport infrastructure is located is characterized by turbulent flows. Consequently, the Reynolds-averaged Navier–Stokes (RANS) equations in steady state along with a turbulence model were solved in order to predict the aerodynamic coefficients acting on the bus by using the finite-volume method (FVM). In this work, a steady state analysis is applied instead of transient analysis as the latter is not need to achieve the objectives of the study. In addition, the computational cost and CPU time are considerably higher for unsteady simulations compared to the steady approach. For example, in turbomachinery applications, large eddy simulations (LESs) need approximately 5000 times the amount of computational time needed for a steady analysis which uses RANS (Gourdain, Gicquel, & Collado, 2012). The flow field around a vehicle is unsteady and very complex when incorporating various time and length scales. Therefore, if the study requires high accuracy in the result obtained it is necessary to carry out a transient analysis. However, if the goal is to predict which structural configuration more negatively influences vehicle stability, as in the present study, then the steady approach should be accurate enough. Nevertheless, in order to study the effect of using a steady approach instead of an unsteady one, the aerodynamic coefficients acting on the bus were obtained by both procedures for the box bridge deck (section 4). The RANS equations govern the fluid movement through the three fundamental conservation principles: mass, momentum and energy. On the other hand, the turbulence models help to estimate the Reynolds stress and, consequently, to close the equation system composed by the RANS equations. Among the potential turbulence models that can be implemented in CFD code, the bus aerodynamic coefficients were obtained for three of them: Spalart–Allmaras (Spalart & Allmaras, 1994), standard $k - \varepsilon$ (Lauder & Spalding, 1974) and shear stress transport (SST) $k - \omega$ (Menter, 1994). The near-wall region is solved by different methods according to the turbulence model applied. The Spalart–Allmaras model uses a formulation that automatically blends from a viscous sublayer formulation to a logarithmic formulation based on the value of y^+ . Therefore, this wall treatment can be used to solve the near-wall region with independence of the refinement level of the grid. As for the standard $k - \varepsilon$ turbulence models, an enhanced wall treatment was chosen to solve

the near-wall region instead of a standard wall function because of the higher accuracy of this method in predicting the air flow behavior in the near-wall region. This approach combines a two-layer model with the so-called enhanced wall functions. If the near-wall mesh is fine enough to be able to resolve the viscous sublayer ($y^+ \approx 1$) then a two-layer approach is applied, while if the mesh is coarse then enhanced wall functions are used. The enhanced wall functions formulate the law of the wall as a single law for the entire wall region (viscous sublayer, buffer region and fully-turbulent outer region) by blending the linear (laminar) and logarithmic (turbulent) law-of-the-wall. This feature allows the near-wall regions to be solved for different grid densities. The main difference between the standard $k - \varepsilon$ model and the SST $k - \omega$ model regarding the near-wall treatment applied consists of the fact that the ω -equation can be solved through the viscous sublayer without the need for the two-layer approach that has to be used with the ε -equation. The results obtained for each turbulence model studied are presented in section 3. Detailed information on the RANS equations and the turbulence models equations can be found in the FLUENT user manual.

In the FVM, the fluid domain is divided into a finite number of cells with nodal points. The shape and position of control volumes with respect to grid cells is defined according to a cell-centered scheme. Therefore, the control volumes are equal to the grid cell both in shape and position. These control volumes are delimited by the nodal point in the grid and the variable values are stored at the centroids of the grid cells. The governing partial differential equations are integrated over the control volumes to evaluate the convective and viscous fluxes as well as the source terms. Then, the equations in integral form are discretized and thus transformed into algebraic equations by the application of quadrature formulae. These algebraic equations contain the values of variables and fluxes at the control volume faces which are expressed in terms of the center values via the interpolation scheme.

In the present study, a second-order upwind scheme was used for the moment equations and the turbulence quantities and a second-order scheme was used for the pressure equations during spatial discretization. The variable gradients between the cell centroids were evaluated by the least squares cell-based method. The semi-implicit method for pressure-linked equations (SIMPLE) algorithm (Patankar & Spalding, 1972) was used to solve the pressure–velocity coupling. Finally, the algebraic equation system was solved using an iterative method.

2.3. Boundary conditions and grid

The 3D domain, which contains the regions of air around both the bus and the bridge deck models, has a cross section with the same dimensions as the wind tunnel section of the Polytechnic University of Milan (14 m × 4 m; Bocciolone, Cheli, Corradi, Muggiasca, & Tomasini, 2008). The upstream and downstream distance between the bridge deck and the boundary surfaces (Figure 3) exceeded the minimum values established under European regulation EN 14067-6:2010. These distances are expressed as a function of the obstacle height H_{obs} (the distance between the top surface of the bus and the bottom surface of the bridge deck). The numerical simulation was carried out with a still bus model without reproducing the relative movement between the bus and the bridge deck because the computational cost would have been greater, and vehicle motion has no significant influence on the force coefficients according to Bocciolone et al. (2008). In order to obtain the aerodynamic coefficients for each value of the yaw angles studied when the bus model is located on the three bridge deck types, the bus and bridge deck were rotated together (Figure 4).

The domain was divided into two subdomains (the far domain and the near domain; Figure 5) to build a finer grid in the air region close to the bus model where strong gradients of the flow variables originate. In the near domain, two types of cells were used: wedge cells were used for the air regions near the bus surface by applying an inflation control and tetrahedral cells were used for the other regions, while in the far domain only tetrahedral cells were used. The wedge grid performed

well in solving the near-wall region problem, which can be subdivided into three layers: the viscous sublayer, the buffer layer and the log-law region. A total of ten inflated layers of wedge with a growth rate of 1.1 make up the wedge grid, the thickness of the first layer being set to obtain a y^+ not exceeding 1, using the following formula:

$$y^+ = \frac{u_\tau \cdot y}{\nu}, \quad (4)$$

where y^+ is the dimensionless distance from the wall related to the distance from the wall y , u_τ is the shear velocity (the value of the friction velocity obtained from the experimental wind profile) and ν is the kinematic viscosity.

A finer grid was built for both the air region close to the curved surface and the small gap of air between walls by using curvature and proximity controls. The boundary condition setup is as follows (Madenci & Guven, 2015; Moaveni, 2014; Tu, 2013):

- Inlet velocity: A uniform profile of 13.5 m/s was defined for the flow velocity U (see Figure 3), and $V, W = 0$ (the components of wind velocity in the y - and z -directions are zero). The turbulent length scale l and turbulence intensity I are ~ 30 m (full-scale value) and 6%, respectively, according to experimental conditions (Dorigatti et al., 2012). The flow is incompressible and subsonic (Versteeg & Malalasekera, 2007):

$$Ma = \frac{U}{c} = \frac{13.5 \text{ m/s}}{340 \text{ m/s}} = 0.04 \ll 0.3 \Rightarrow \nabla \cdot \vec{u} = 0. \quad (5)$$

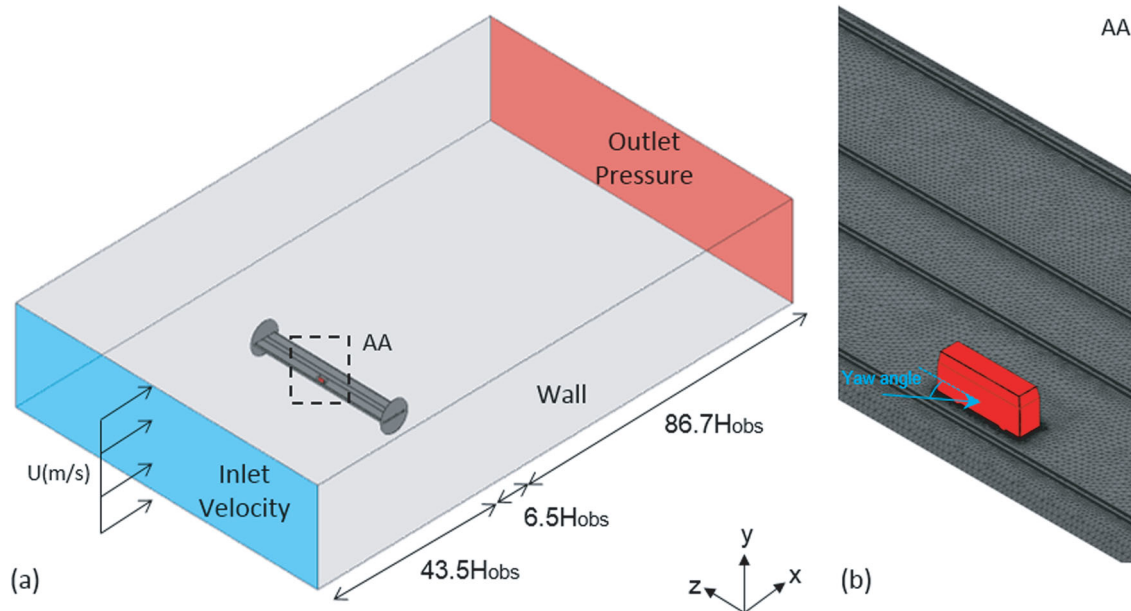


Figure 3. (a) Geometrical model of the numerical domain and boundary conditions, and (b) bus model on the bridge deck for the numerical simulation.

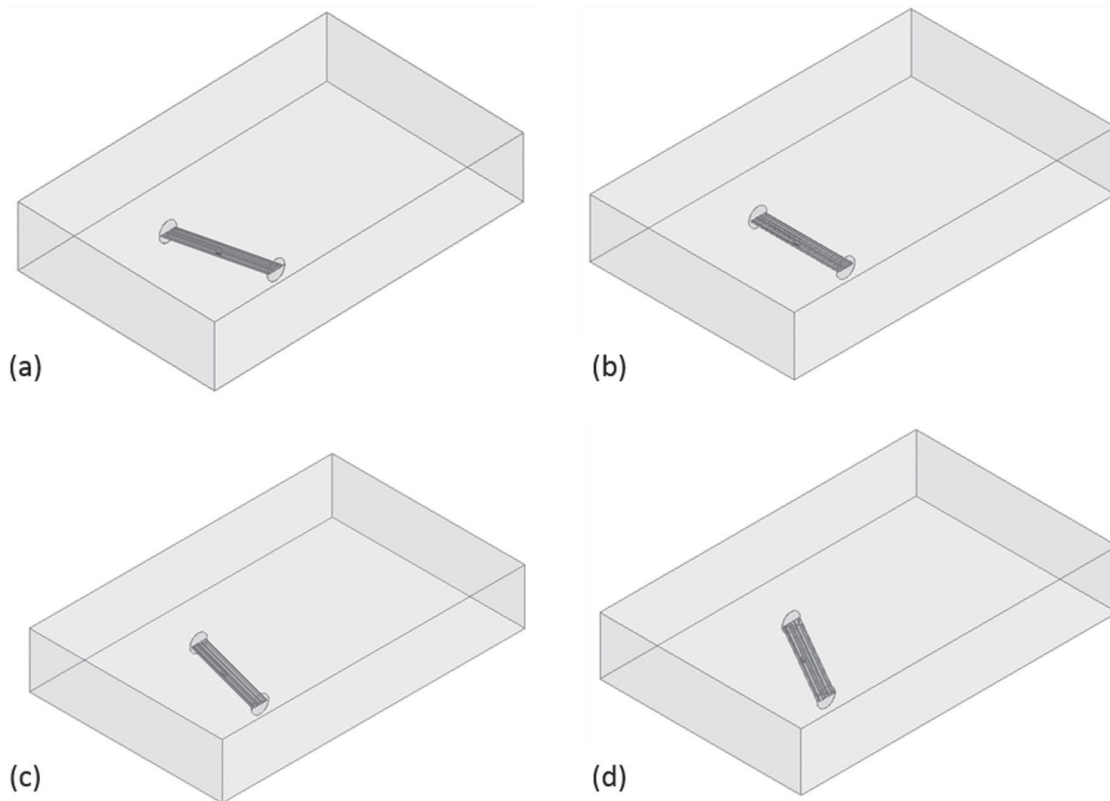


Figure 4. Yaw angle positions studied in the numerical simulation: (a) 75°, (b) 90°, (c) 105°, and (d) 120°.

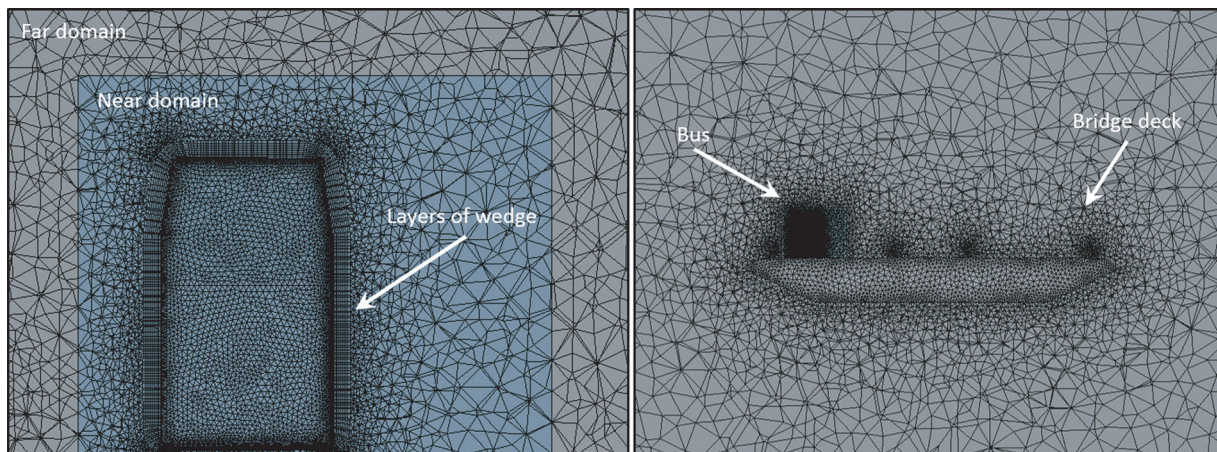


Figure 5. View of the grid employed for the different regions of the domain.

- Outlet pressure: The relative pressure $p = 0$. The normal gradients of all variables were set equal to zero (Neumann boundary condition). Under back flow conditions, the average turbulence intensity I and turbulent length scale l were assigned the inlet boundary condition values.
- Solid walls: A non-slip condition ($U, V, W = 0$) was adopted on the solid surfaces of the domain. The roughness height was set to a null value, therefore the boundary surface behaves as a smooth surface.

3. Grid size and turbulence closure model

The spatial discretization error can be decreased by diminishing the cell size but a smaller cell size requires an increased number of cells in the grid and thus increased computational cost. Therefore, a grid-size independence study was carried out to avoid wasting computational power. In particular, the aerodynamic coefficients acting on the bus located on the box bridge deck with a yaw angle of 90° were obtained for four grid sizes of 13.4,

16.2, 19.1 and 22.8 million cells. The distribution of elements by type for the grid size built is shown in Table 1. In the grid-size sensitivity analysis, the SST $k-\omega$ model was used instead of the Spalart–Allmaras and standard $k-\epsilon$ models due to this model having more rigorous mesh-refinement requirements compared to the others.

The different levels of refinement were obtained by applying a size control function on the near domain, which is the air region where the variable gradients are stronger and a smaller cell size is likely required (Figure 6). The results indicate that the aerodynamic coefficients acting on the bus are independent of the grid size for the four sizes examined here (Figure 7). Thus, the grid setup defined for 13.4 million cells was applied to the other numerical simulations.

Table 1. Distribution of elements for several grid sizes.

Grid size (million)	Tetrahedrons (%)	Wedges (%)
13.4	94.02	5.98
16.2	95.05	4.95
19.1	89.70	10.30
22.8	96.48	3.52

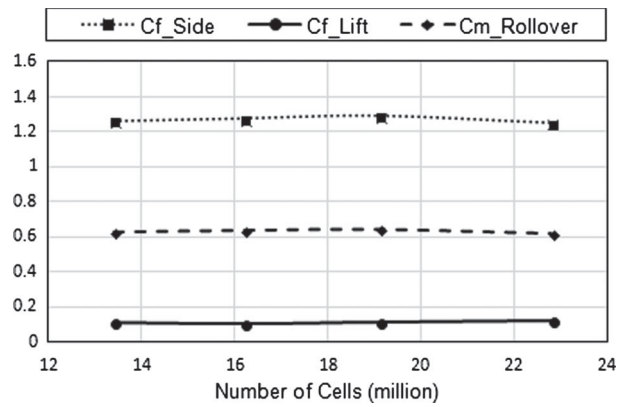


Figure 7. Influence of the grid size on the aerodynamic coefficients of the bus for the box bridge deck.

The grid size varies with the yaw angle studied for the three types of bridge deck. Specifically, the maximum variation of grid size with the yaw angle with respect to the grid size for a 90° yaw angle in each bridge deck type, is shown in the Table 2.

Then, the relative errors between the aerodynamic coefficients obtained by the three turbulence models

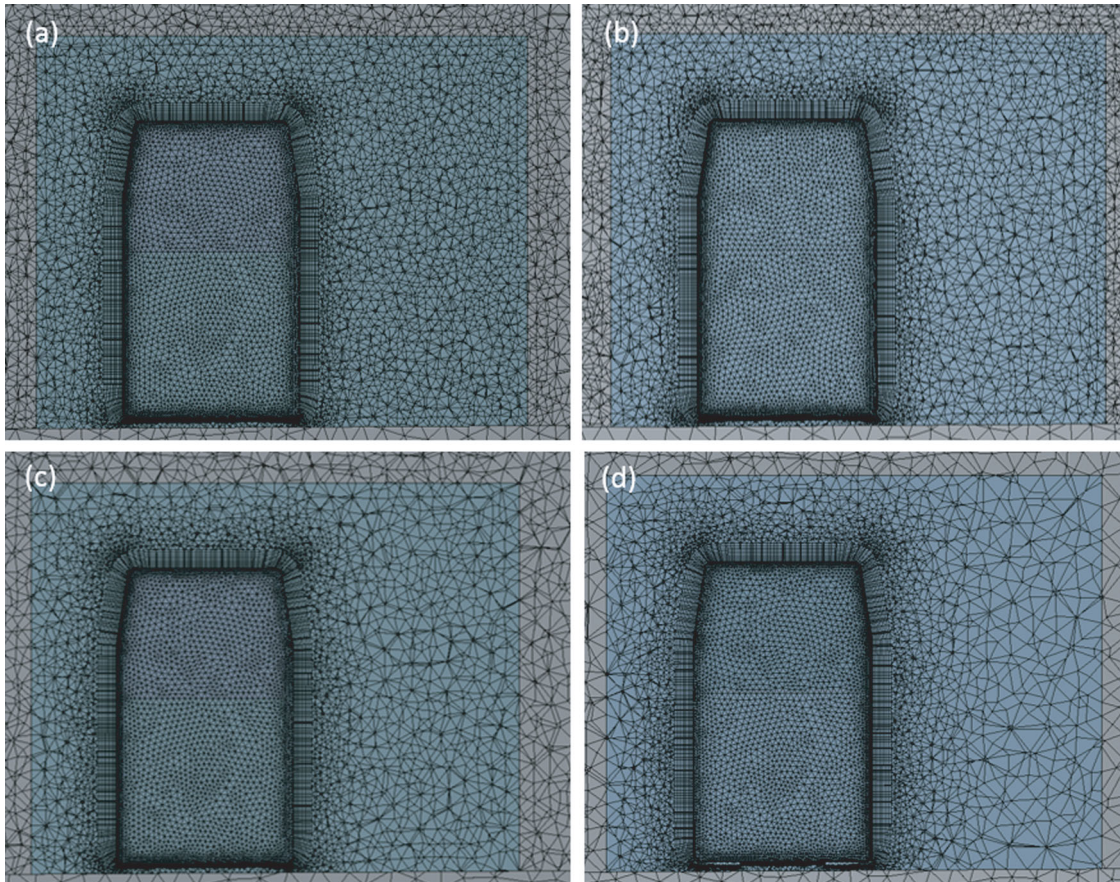


Figure 6. Grid in the region where the refinement was applied for the following grid sizes: (a) 22.8 million, (b) 19.1 million, (c) 16.2 million, and (d) 13.4 million.

Table 2. Yaw angle where the maximum variation of grid size with respect to 90° of yaw angle was obtained for each bridge deck.

Bridge deck	Yaw angle (°)	Maximum variation of grid size (million)
Box	75	1.0
Board	120	0.4
Girder	120	1.9

(Spalart–Allmaras, standard $k - \varepsilon$ and SST $k - \omega$) and by the experiment (Dorigatti et al., 2012) were determined in order to select the turbulence model.

The lowest relative error in the three coefficients was obtained with the SST $k - \omega$ model (Table 3); therefore, this model was used in the other scenarios. The lift coefficient exhibits the highest relative error; this could be because the components that were used to link the balance and the bus model in the experimental test were not defined in the numerical simulation, since these geometric details are not indicated in Dorigatti et al. (2012). Specifically, the experimental value of the lift coefficient is lower than the value obtained by the numerical model due to the smaller air gap between the bus model and the road surface, which is a consequence of the components used to link the bus model and the balance in the experimental test. This smaller gap causes higher values of velocity and lower values of static pressure in the air flow under the bus and consequently the lift force diminishes in comparison to the numerical values. On the other hand, these components are actually supposed to modify the air flow through the gap between the bus and road surface with respect to real conditions.

Table 3. Relative error for the aerodynamic coefficients as a function of the turbulence model for the box bridge deck.

Turbulence model	Aerodynamic coefficients		
	Cf_Side	Cf_Lift	Cm_Rollover
$k - \varepsilon$	0.18	7.00	0.12
SST $k - \omega$	0.01	3.75	0.05
Spalart–Allmaras	0.25	6.50	0.23

The results of the numerical models can be considered accurate enough to reach the objective set for this study for the following reasons: the weight of the lift coefficient on the rollover coefficient is less than the weight of the side coefficient on the rollover coefficient; the lift force values are significantly lower than the side force values and consequently when the difference between the numerical and experimental values are expressed in terms of relative error, the error relative to the lift coefficients is significant higher than the other errors; and finally the relative error of the side coefficient is low enough to rely on this value.

One of the main characteristics of the SST $k - \omega$ model is its good performance in solving low Reynolds flows such as those present in near-wall regions (ANSYS, 2013; Tu, 2013). Many authors recommend that the SST $k - \omega$ model should be used in place of the standard $k - \varepsilon$ model as the first choice (Andersson et al., 2011).

4. Comparison between unsteady and steady aerodynamic coefficients

An unsteady numerical simulation with the SST $k - \omega$ model was carried out prior to the use of the steady approach for the proposed cases. Thus, the box bridge deck was used to calculate the aerodynamic coefficients of the bus by applying a steady approach as unsteady. The non-dimensional time step was set as $\Delta t^* = \Delta t \cdot U_\infty / H = 0.097$, where H is the height of bus as in Ai and Mak (2015), keeping a Courant–Friedrichs–Lewy (CFL) number of less than 1 in the most of the cells of regions with flow detaching. The simulations were run for a total time of 2712 Δt^* , the time required by the air flow to cover three times the domain. The first 556 Δt^* were not considered when calculating the average values of the aerodynamic coefficient because the values were not stable. Figure 8 shows the relationships between the average values of the aerodynamic coefficients and the yaw angle for the two numerical approaches (steady

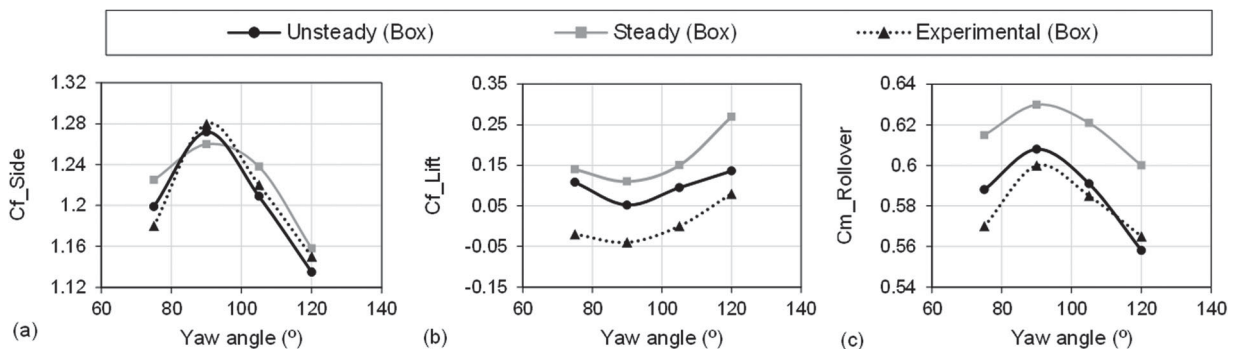


Figure 8. Comparison between the aerodynamic coefficients obtained by the steady and unsteady approaches and the experiment in Dorigatti et al. (2012): (a) side force, (b) lift force, and (c) rollover moment.

and unsteady) and the experimental test (Dorigatti et al., 2012). The unsteady analysis exhibits values of aerodynamic coefficients closer to experimental measurements; however, the variations in the aerodynamic coefficients with the yaw angle are quite similar for both approaches. Therefore, the steady approach allows the obtention of accurate enough trends with regard to the objectives of this study.

5. Design of experiment (DOE) methodology

In order to study the effect of the box deck design parameters on the aerodynamic loads acting on the bus, a sensitivity analysis and a DOE analysis were carried out. The results from the DOE analysis enabled the optimization of the box deck configuration. A central composite design (CCD) was chosen to determine the number of cases required to perform the study as a part of the DOE methodology (Del Coz Díaz, Serrano López, López-Colina Pérez, & Álvarez Rabanal, 2012; Myers, Montgomery, & Anderson-Cook, 2009). Then, the output and input variables were selected and the ranges of values for the input variables were defined. These ranges of values were used by the central composite design in order to propose the values of input variables in the cases which will be solved. Each combination of input variables requires that the output variables are calculated by means of a new volume finite analysis. A response surface model is obtained according to the second-order polynomial regression model set and the results from the DOE study. The response surface is an explicit approximation function which expresses the output data as a function of input data by the fitting algorithm indicated in the DOE methodology.

As part of the DOE procedure, the higher-order derivatives are evaluated from the results generated for each design point, and the order of the derivatives indicates the order of the approximation expressions. The second-order model applied in the present work considering two input variables can be written as follows:

$$Y = \lambda_0 + \lambda_1 x_1 + \lambda_2 x_2 + \lambda_{11} x_1^2 + \lambda_{22} x_2^2 + \lambda_{12} x_1 x_2 + \text{error}, \quad (6)$$

where Y is the predicted response variable, the instances of x are the factors or input variables and the instances of λ s are the regression coefficients. There is one two-way interaction term according to $p(p-1)/2 = 2 \times 1/2 = 1$, and there are two quadratic terms and two linear terms. The regression coefficients λ were calculated by the ordinary least squares (OLS) procedure, where the OLS estimator can be written as:

$$\vec{\lambda}_{\text{OLS}} = (\vec{X}^T \vec{X})^{-1} \vec{X}^T \vec{Y} \quad (7)$$

where \vec{X} is the extended designed matrix for the input variables including the coded levels and \vec{Y} is a column vector of output variable values obtained for the specify points in the DOE. The input variables over their variation range (maximum, minimum and current value) and the output variables are as follows:

- Input variables (Figure 1): the height of the deck box h and the angle of deck box θ . The height of deck box varies from 25 mm to 92.5 mm (in full scale from 1 m to 3.7 m) with a starting design value of 58.75 mm (2.35 m in full scale). The deck box angle varies from 15° to 45° with a starting design value of 30°.
- Output parameters: the aerodynamic coefficients associated with the side force, lift force and rollover moment.

6. Results and discussion

In this section, the influence of both the bridge deck configuration and the wind fence slope on aerodynamic loads which contribute to rollover accidents under crosswind conditions is shown and discussed.

6.1. Effect of the bridge deck configuration

In order to study the effect of the bridge deck type on the stability of a bus model, the aerodynamic coefficients of the bus were obtained for three types, as detailed in section 2. Figure 9 illustrates the aerodynamic coefficients acting on the bus located on the three bridge decks considered for four yaw angle values: 75°, 90°, 105° and 120°. In order to obtain the aerodynamic coefficients for each value of yaw angle, the bus and the bridge deck were rotated together. While the side and rollover coefficients approach the highest values for a yaw angle of 90°, the lift coefficient approaches the lowest values. The side and rollover coefficients show a similar trend with respect to the yaw angle due to the stronger influence above the rollover moment by the side force compared to the lift force. However, the lift coefficient exhibits a behavior that is in opposition to the other coefficients, as in Dorigatti et al. (2012). The side and rollover coefficients diminish when the yaw angle moves away from the perpendicular to the traffic direction and the lift coefficient increases. Moreover, the differences between aerodynamic coefficients for the three bridge deck types are quite small, but the board type seems to have more of a negative influence on bus stability than the other types for most of the yaw angle values. A sample of numerical results relative to static pressure and wind velocity in the air region around the bus for a yaw angle of 90° is illustrated in

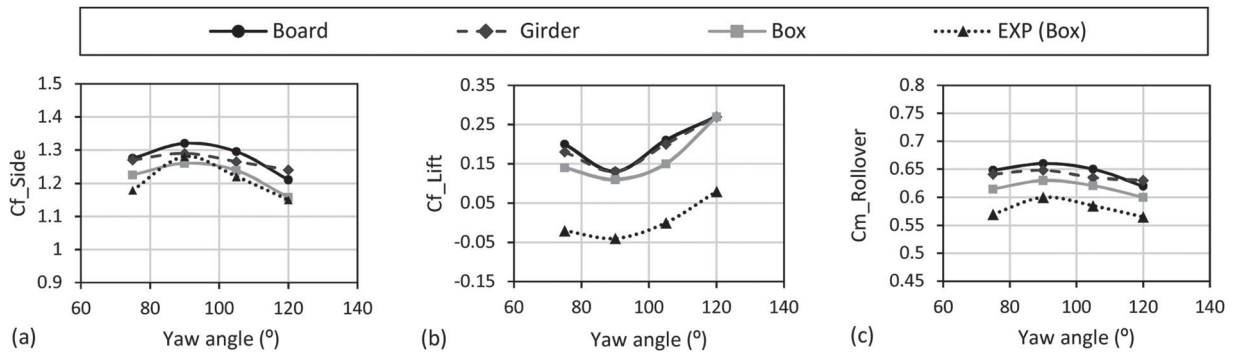


Figure 9. Relationships between the aerodynamic coefficients obtained by the CFD program and Dorigatti et al. (2012), and the yaw angle for different bridge decks: (a) side force, (b) lift force, and (c) rollover moment.

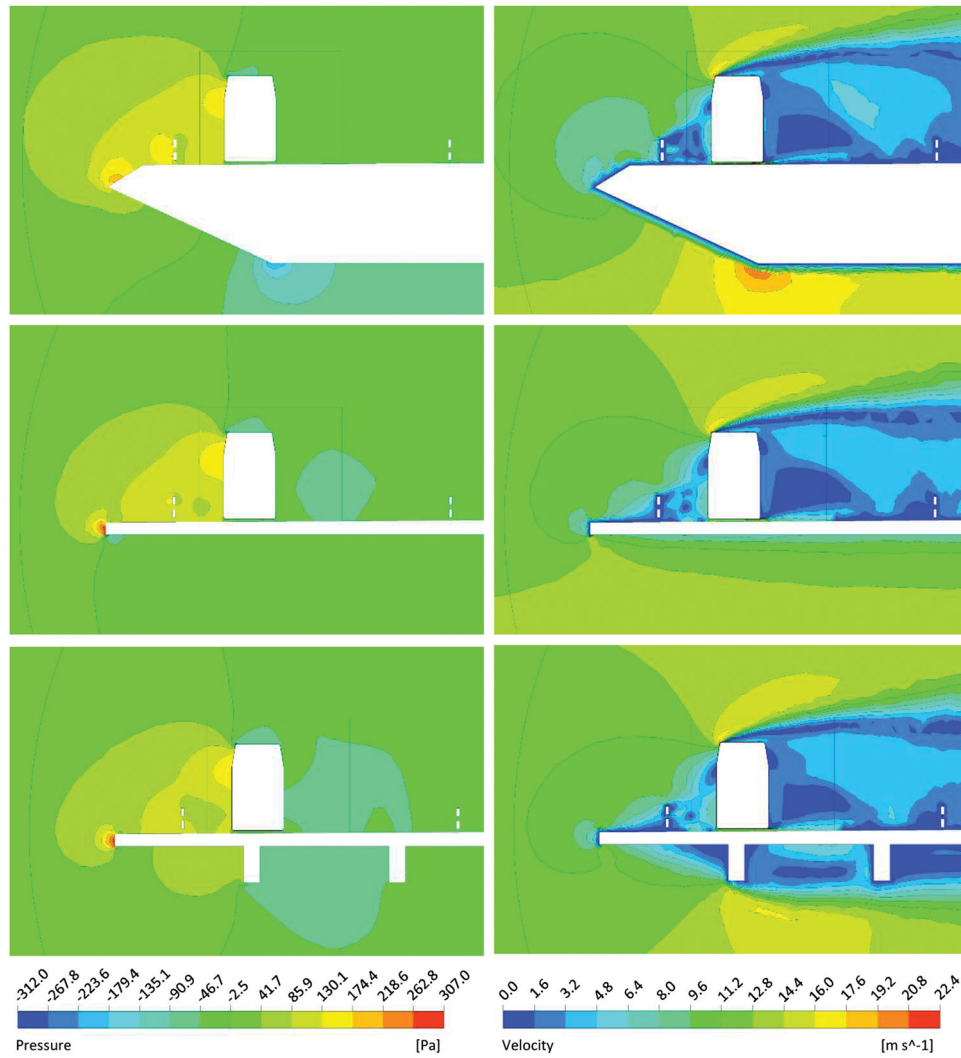


Figure 10. Pressure and wind velocity contours calculated for the three types of bridge deck with a yaw angle of 90°.

Figure 10. The results indicate that there is not a great difference between the bridge deck types with respect to the air flow velocity around the bus; however, it is interesting to note that the bus stability could be improved if the bridge deck model caused a higher perturbation on the

air flow hitting the bus. The stronger gradients of pressure and velocity in the air region below the bridge decks (Figure 10) are caused by the girder and box types, and these are the bridge decks where higher values of rollover coefficient are obtained.

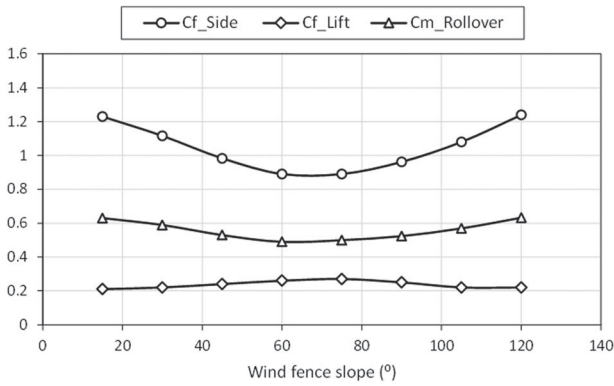


Figure 11. Relationship between the aerodynamic coefficients of the bus and the wind fence slope for the box deck under crosswind conditions.

6.2. Effect of the wind fence slope

In this section, the relationships between the wind fence slope (β angle) and the aerodynamic coefficients of the bus are studied under crosswind conditions (yaw angle of 90°). The most important parameter with

respect to crosswind stability is the rollover moment coefficient (Schober, Weise, Orellano, Deeg, & Wetzell, 2010), therefore the wind fence performance was evaluated through the reduction of this coefficient. Similar behavior is exhibited in the side force coefficient and the rollover moment coefficient versus the wind fence slopes (Figure 11), where two regions can be distinguished. In the first region, both coefficients decrease from a wind fence slope of 15° to 60° , where the minimum values are reached and remain fairly constant until 75° , at which point the coefficients begin to increase. The lift coefficient exhibits the opposite trend to the rollover and side coefficients wherein the maximum value of the lift coefficient is approached for a wind fence slope of 75° (Figure 11). Among the slope angles of wind fence studied, 60° is the position where the minimum value of rollover coefficient is obtained. For this slope angle value, a lower number of streamlines hit on the top zone of the windward surface of the bus in comparison with other values of wind fence slope, which result in a reduction of the rollover coefficient of the bus (Figure 12). Specifically, this articulating wind fence reduces the rollover coefficient in relation to the crash barrier by a maximum value of 22% (a wind

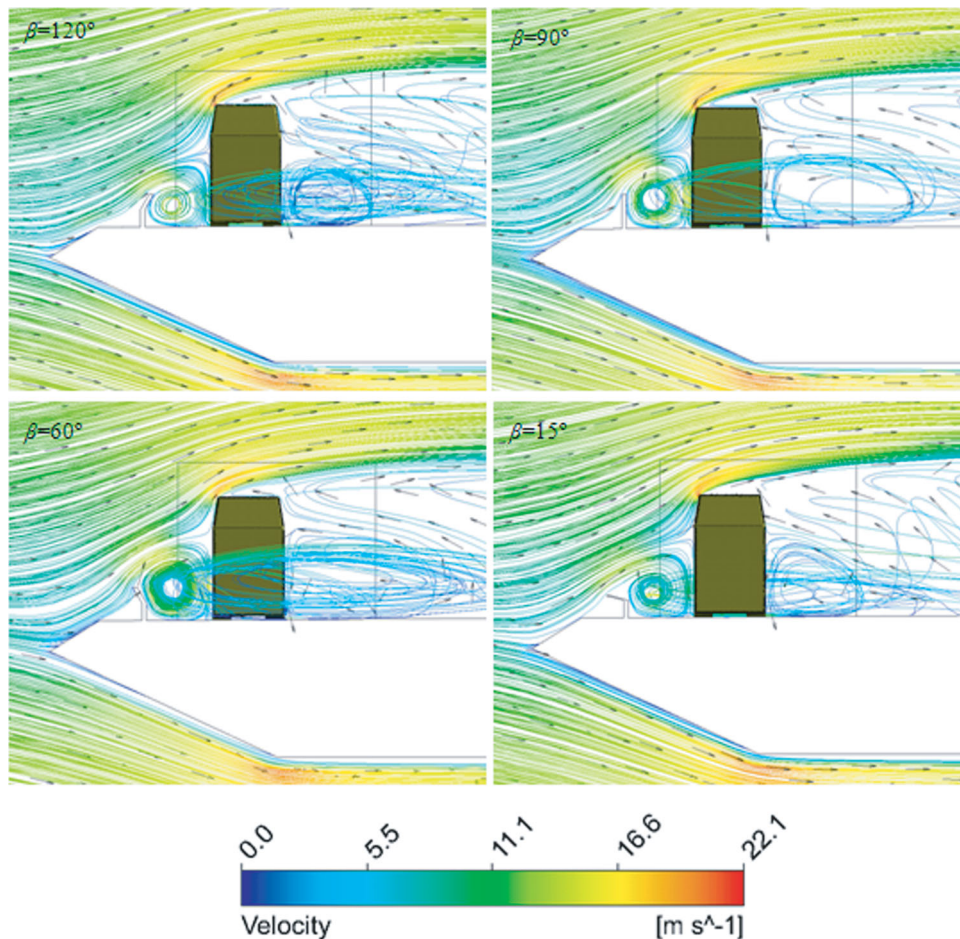


Figure 12. Streamlines of velocity field around the bus for four values of wind fence slope angle β .

fence slope angle of 60°). While the side coefficient of the bus was higher when the crash barrier was installed, the lift coefficient was lower in comparison with the case of an articulating wind fence. This difference in lift coefficient is due in part to the reduced air flow through the gap between the bus and the road for the articulating wind fence, and as a result the pressure is higher in the air region under the bus, which causes an increase in the pressure difference between the top and underneath surfaces of the bus.

6.3. Effect of the box bridge deck configuration

The influence of two geometrical parameters of the box bridge deck on the bus aerodynamics was studied by solving nine numerical models. A converged solution was reached when the following requirements were fulfilled: the scaled residuals of all the variables were less than $1 \cdot 10^{-5}$, the net flux imbalance was less than 1% of the smallest flux through the domain boundary and the monitored aerodynamic coefficient keeps constant up to three decimals (ANSYS, 2013). In order to carry out the simulations, a server with a CPU Intel Xeon 5630@2.53 GHz (8 processors) with 64 GB RAM and a 4 TB hard disk were used, running the Windows Server 2003 operating system. The geometry input parameters described in section 4 were coded into three values (-1, 0, 1) by applying this expression (Montgomery, 2013):

$$x_{\text{coded}} = \frac{x - (x_{\text{low}} + x_{\text{high}})/2}{(x_{\text{low}} - x_{\text{high}})/2}. \quad (8)$$

The response surface models fitted with the results obtained after solving the cases proposed by the design of experiment are plotted in Figure 13. These graphs show the maximum variation of the aerodynamic coefficients of the bus caused by the effect of the deck box height and deck box angle within a predetermined range of values. The adjusted coefficients of determination, R_{adj}^2 , related to the response surface models are 0.79 for the lift coefficient, 0.76 for the side coefficient and 0.69 for the rollover coefficient. Among the cases solved, the best configuration of the box deck is the one for which the minimum coefficient of rollover is reached. Specifically, a minimum value of 0.628 for the rollover coefficient is obtained for a box angle of 45° (+1 coded value) with a height of 92.5 mm (+1 coded value) (Figure 13). However, the influence of these parameters on both the rollover coefficient and the side coefficient is quiet modest because the response variation with respect to the average value is below 5%. In the case of the lift coefficient, it reaches a maximum variation of 16% but its influence on the

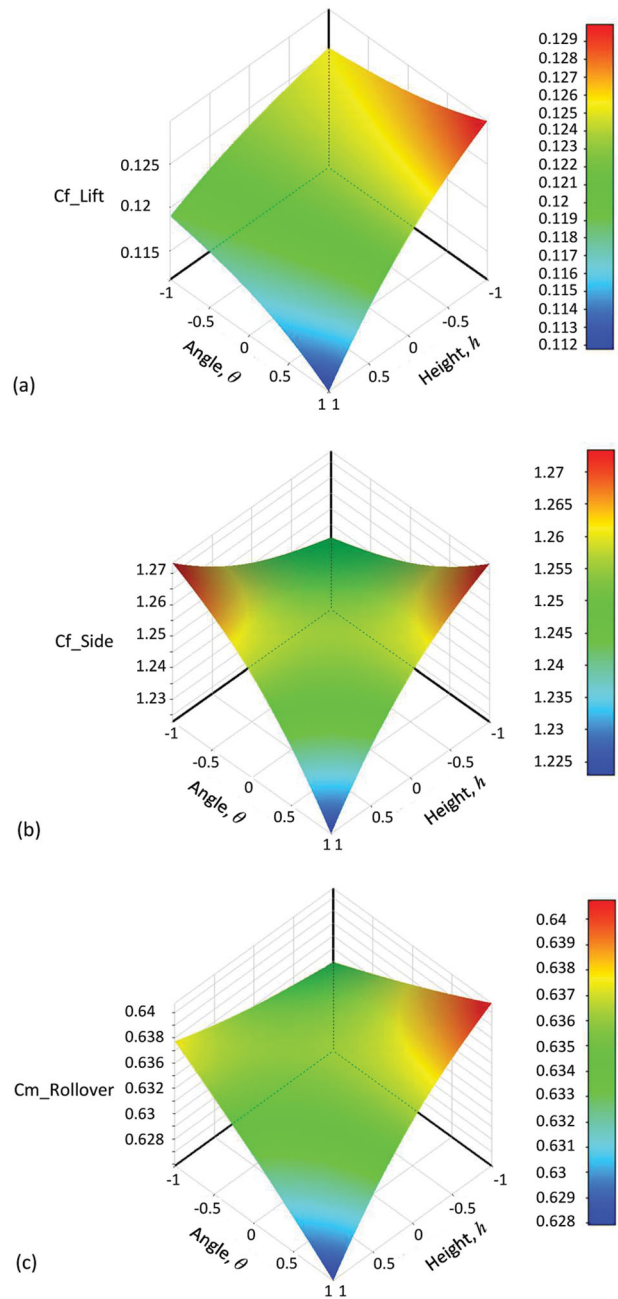


Figure 13. Response surfaces relating to the geometrical parameters of the box deck (box angle and box height) for the aerodynamic coefficients: (a) lift force, (b) side force, and (c) rollover moment.

rollover coefficient is quite a bit less than the influence of the side coefficient.

In addition, a sensitivity study was carried out for the independent assessment of this geometrical parameter on the aerodynamic coefficient acting on the bus. The results indicate that the height of the box significantly influences both the rollover coefficient and the lift coefficient, while the angle of box does not correlate with any aerodynamic coefficient (Figure 14). The effect of the height parameter

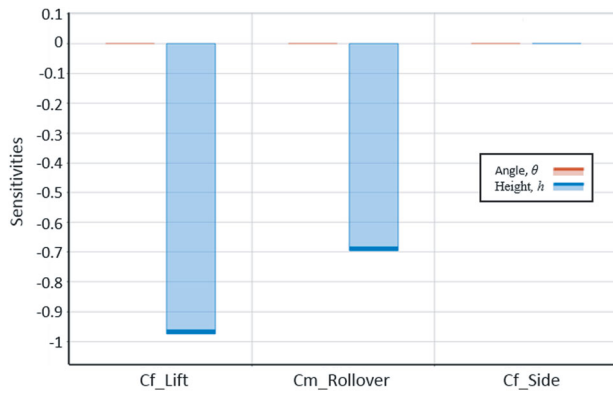


Figure 14. Global sensitivity values between the aerodynamic coefficients of the bus and the geometrical parameters of the box deck.

above the rollover coefficient is due to the negative value of the sensitivity between this parameter and the lift coefficient, because the side coefficient is not affected by the height of the box. To sum up, the risk of rollover accident does not strongly depend on this geometry parameter of the box deck.

7. Conclusions

In this work, a methodology has been developed to help identify scenarios on roads where crosswind conditions have a greater negative impact on traffic safety. Authorities will be able to use this information to decide, with more precise criteria, on issues such as in which infrastructures it is most necessary to install a wind fence and when bridges must be closed due to strong crosswinds. In addition, a new approach which consists in improving traffic safety by modifying the structural configuration of the bridge decks was undertaken.

The main findings from the quantitative results are as follows:

- Of the three types of bridge deck tested, the board type has a slightly greater negatively influence on bus stability than the other two types in the yaw angle range studied (75° to 120°).
- In terms of the effect of the wind fence slope angle on the aerodynamic coefficients of the bus, the minimum value of rollover moment coefficient was obtained for an angle of 60° with respect to the horizontal plane.
- The articulating wind fence was revealed as a better option for protecting vehicles from crosswinds than the crash barrier. Specifically, this wind fence model reduces the rollover coefficient in relation to the crash barrier by a maximum value of 22%.
- The rollover coefficient acting on the bus exhibits variations below 5% for the two geometry parameters of

the box bridge deck studied; therefore, it can be stated that the risk of rollover accidents is not significantly affected by these parameters.

- With regard to numerical setup, the best fit to the experimental data was obtained by using the SST $k-\omega$ turbulence model.
- The FVM has proved to be a powerful tool for solving the RANS equations in combination with the SST $k-\omega$ turbulence model.
- In the case of the box bridge deck, the unsteady approach was found to be more accurate than the steady approach. However, the trends in the graphs are relatively similar for both approaches.
- In order to carry out a more detailed study of the unsteady behavior of the fluids around the bus, it might be interesting to apply other more accurate approaches that require a higher computational cost, such as an LES, a detached eddy simulation (DES) or a scale adaptive simulation (SAS).

Acknowledgements

This work was supported by the OASIS Research Project that was co financed by CDTI (Spanish Science and Innovation Ministry) and developed with the Spanish companies: Iridium, OHL Concesiones, Abertis, Sice, Indra, Dragados, OHL, Geocisa, GMV, Asfaltos Augusta, Hidrofersa, Eipsa, PyG, CPS, AEC and Torre de Comares Arquitectos S.L and 16 research centres. The authors also acknowledge the partial funding with FEDER funds under the Research Project FC-15-GRUPIN14-004. Finally, we also thanks to Swanson Analysis Inc. for the use of ANSYS University Research programs as well as the Workbench simulation environment.

Disclosure statement

No potential conflict of interest was reported by the authors.

ORCID

A. Alonso-Estébanez <http://orcid.org/0000-0003-2480-1980>

J. J. Del Coz Díaz <http://orcid.org/0000-0002-4288-3839>

F. P. Álvarez Rabanal <http://orcid.org/0000-0002-8011-7246>

P. Pascual-Muñoz <http://orcid.org/0000-0001-9181-4744>

References

- Ai, Z. T., & Mak, C. M. (2015). Large-eddy simulation of flow and dispersion around an isolated building: Analysis of influencing factors. *Computer and Fluids*, 118, 89–100. doi:10.1016/j.compfluid.2015.06.006
- Andersson, B., Andersson, R., Hakansson, L., Mortensen, M., Rahman, S., & Berend, V. W. (2011). *Computational fluid dynamics for engineers*. New York, USA: Cambridge University Press.
- ANSYS. (2013). *Fluent manual release 15.0*. Canonsburg, PA: ANSYS Inc. <https://uiuc-cse.github.io/me498cm-fa15/lessons/fluent/refs/ANSYS%20Fluent%20Theory%20Guide.pdf>

- Argentini, T., Ozkan, E., Rocchi, D., Rosa, L., & Zasso, A. (2011). Cross-wind effects on a vehicle crossing the wake of a bridge pylon. *Journal of Wind Engineering and Industrial Aerodynamics*, 99, 734–740. doi:10.1016/j.jweia.2011.01.021
- Baker, C. J., & Reynolds, S. (1992). Wind-induced accidents of road vehicles. *Accident Analysis and Prevention*, 24, 559–575. doi:10.1016/0001-4575(92)90009-8
- Bettle, J., Holloway, A. G. L., & Venart, J. E. S. (2003). A computational study of the aerodynamic forces acting on a tractor-trailer vehicle on a bridge in cross-wind. *Journal of Wind Engineering and Industrial Aerodynamics*, 91, 573–592. doi:10.1016/S0167-6105(02)00461-0
- Bocciolone, M., Cheli, F., Corradi, R., Muggiasca, S., & Tomasini, G. (2008). Crosswind action on rail vehicles: Wind tunnel experimental analyses. *Journal of Wind Engineering and Industrial Aerodynamics*, 96, 584–610. doi:10.1016/j.jweia.2008.02.030
- Charuvisit, S., Kimura, K., & Fujino, Y. (2004). Effects of wind barrier on a vehicle passing in the wake of a bridge tower in cross wind and its response. *Journal of Wind Engineering and Industrial Aerodynamics*, 92, 609–639. doi:10.1016/j.jweia.2004.03.006
- Cheli, F., Corradi, R., Rocchi, D., Tomasini, G., & Maestrini, E. (2010). Wind tunnel tests on train scale models to investigate the effect of infrastructure scenario. *Journal of Wind Engineering and Industrial Aerodynamics*, 98, 353–362. doi:10.1016/j.jweia.2010.01.001
- Cheli, F., Corradi, R., Sabbioni, E., & Tomasini, G. (2011). Wind tunnel tests on heavy road vehicles: Cross wind induced loads—Part 1. *Journal of Wind Engineering and Industrial Aerodynamics*, 99, 1000–1010. doi:10.1016/j.jweia.2011.07.009
- Chen, G., Wang, W., Sun, C., & Li, J. (2012). 3D numerical simulation of wind flow behind a new porous fence. *Powder Technology*, 230, 118–126. doi:10.1016/j.powtec.2012.07.017
- Cheung, M. M. S., & Chan, B. Y. B. (2010). Operational requirements for long-span bridges under strong wind events. *Journal of Bridge Engineering*, 15, 131–143. doi:10.1061/(ASCE)BE.1943-5592.0000044
- Del Coz Díaz, J. J., Serrano López, M. A., López-Colina Pérez, C., & Álvarez Rabanal, F. P. (2012). Effect of the vent hole geometry and welding on the static strength of galvanized RHS K-joints by FEM and DOE. *Engineering Structures*, 41, 218–233. doi:10.1016/j.engstruct.2012.03.050
- Dorigatti, F., Sterling, M., Rocchi, D., Belloli, M., Quinn, A. D., Baker, C. J., & Ozkan, E. (2012). Wind tunnel measurements of crosswind loads on high sided vehicles over long span bridges. *Journal of Wind Engineering and Industrial Aerodynamics*, 107–108, 214–224. doi:10.1016/j.jweia.2012.04.017
- EN 14067-6:2010. European Standard. Railway applications – Aerodynamics – Part 6: Requirements and test procedures for cross wind assessment. CEN, 2010.
- Gourdain, N., Gicquel, L. Y. M., & Collado, E. (2012). Comparison of RANS and LES for prediction of wall heat transfer in a highly loaded turbine guide vane. *Journal of Propulsion and Power*, 28, 423–433. doi:10.2514/1.B34314
- Guo, W. H., & Xu, Y. L. (2006). Safety analysis of moving road vehicles on a long bridge under crosswind. *Journal of Engineering Mechanics*, 132, 438–446. doi:10.1061/(ASCE)0733-9399(2006)132:4(438).
- Hibino, Y., Shimomura, T., & Tanifuji, K. (2010). Full-Scale experiment on the behavior of a railway vehicle being subjected to lateral force. *Journal of Mechanical Systems for Transportation and Logistics*, 3, 35–43. doi:10.1299/jmtl.3.35.
- Judd, M. J., Raupach, M. R., & Finnigan, J. J. (1996). A wind tunnel study of turbulent flow around single and multiple wind-breaks, part I: Velocity fields. *Boundary-Layer Meteorology*, 80, 127–165.
- Kozmar, H., Butler, K., & Kareem, A. (2009, November). *Aerodynamic loads on a vehicle exposed to cross-wind gusts: An experimental study*. Paper presented in 7th Asia-Pacific Conference on Wind Engineering, APCWE-VII, Taipei, Taiwan.
- Kozmar, H., Procino, L., Borsani, A., & Bartoli, G. (2012). Sheltering efficiency of wind barriers on bridges. *Journal of Wind Engineering and Industrial Aerodynamics*, 107–108, 274–284. doi:10.1016/j.jweia.2012.04.027
- Launder, B. E., & Spalding, D. B. (1974). The numerical computation of turbulent flows. *Computer Methods in Applied Mechanics and Engineering*, 3, 269–289. doi:10.1016/0045-7825(74)90029-2
- Madenci, E., & Guven, I. (2015). *The finite element method and applications in engineering using ANSYS*. New York: Springer.
- Menter, F. R. (1994). Two-equation eddy-viscosity turbulence models for engineering applications. *AIAA Journal*, 32, 1598–1605.
- Moaveni, S. (2014). *Finite element analysis: Theory and application with ANSYS*. New York: Prentice Hall.
- Montgomery, D. C. (2013). *Design and analysis of experiments* (8th ed.). North Carolina, USA: John Wiley & Sons.
- Myers, R. H., Montgomery, D. C., & Anderson-Cook, C. M. (2009). *Response surface methodology: Process and product optimization using designed experiments*. New York: John Wiley & Sons.
- Patankar, S. V., & Spalding, D. B. (1972). A calculation procedure for heat, mass and momentum transfer in three-dimensional parabolic flows. *International Journal of Heat and Mass Transfer*, 15, 1787–1806. doi:10.1016/0017-9310(72)90054-3
- Rocchi, D., Rosa, L., Sabbioni, E., Sbroi, M., & Belloli, M. (2012). A numerical-experimental methodology for simulating the aerodynamic forces acting on a moving vehicle passing through the wake of a bridge tower under cross wind. *Journal of Wind Engineering and Industrial Aerodynamics*, 104–106, 256–265. doi:10.1016/j.jweia.2012.03.012
- Schober, M., Weise, M., Orellano, A., Deeg, P., & Wetzel, W. (2010). Wind tunnel investigation of an ICE 3 endcar on three standard ground scenarios. *Journal of Wind Engineering and Industrial Aerodynamics*, 98, 345–352. doi:10.1016/j.jweia.2009.12.004
- Spalart, P. R., & Allmaras, S. R. (1994). One-equation turbulence model for aerodynamic flows. *Recherche Aérospatiale*, 5–21.
- Sterling, M., Quinn, A. D., Hargreaves, D. M., Cheli, F., Sabbioni, E., Tomasini, G., . . . Morvan, H. (2010). A comparison of different methods to evaluate the wind induced forces on a high sided lorry. *Journal of Wind Engineering and Industrial Aerodynamics*, 98, 10–20. doi:10.1016/j.jweia.2009.08.008
- Sun, Z., Zhang, Y., Guo, D., Yang, G., & Liu, Y. (2014). Research on running stability of CRH3 high speed trains passing by each other. *Engineering Applications of Computational Fluid Mechanics*, 8, 140–157.

- Suzuki, M., Tanemoto, K., & Maeda, T. (2003). Aerodynamic characteristics of train/vehicles under cross winds. *Journal of Wind Engineering and Industrial Aerodynamics*, 91, 209–218. doi:10.1016/S0167-6105(02)00346-X
- Tu, J. (2013). *Computational fluid dynamics*. Oxford, UK: Butterworth-Heinemann.
- Versteeg, H. K., & Malalasekera, W. (2007). *An introduction to computational fluid dynamics: The finite volume method*. Harlow, England: Pearson Education.
- Wang, B., Xu, Y. L., Zhu, L. D., Cao, S. Y., & Li, Y. L. (2013). Determination of aerodynamic forces on stationary/moving vehicle-bridge deck system under crosswinds using computational fluid dynamics. *Engineering Applications of Computational Fluid Mechanics*, 7, 355–368.
- Wang, B., Xu, Y. L., Zhu, L. D., & Li, Y. L. (2014). Crosswind effect studies on road vehicle passing by bridge tower using computational fluid dynamics. *Engineering Applications of Computational Fluid Mechanics*, 8, 330–344.